Dalton Transactions

Accepted Manuscript

ROYAL SOCIETY OF CHEMISTRY

www.rsc.org/dalton

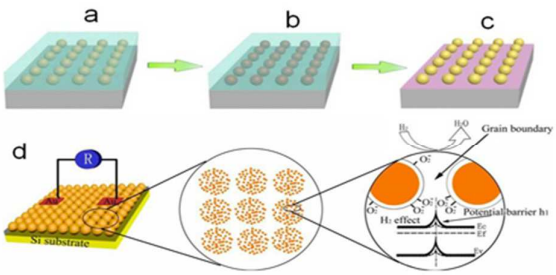

C-doped WO_3 based nanostructures were prepared by taking PS-b-P4VP self-assembly structures as templates and used in room temperature hydrogen response.

Dalton Transactions

ARTICLE

Fabrication of C-doped WO_3 nanoparticle cluster arrays from PS-b-P4VP for room temperature H_2 sensing

Received 00th January 20xx,
Accepted 00th January 20xx

DOI: 10.1039/x0xx00000x

www.rsc.org/

Shu-Juan Liu,*[a,b] Ye Yuan, [a,b] Sheng-Liang Zheng, [a,b] Jing-Huai Zhang, [c] You Wang*[a,b]

Abstract: C-doped WO_3 based room temperature hydrogen sensors including nanoparticle cluster arrays and nanorods were successfully prepared by a PS-b-P4VP template based method. AFM, TEM and XPS are used to characterize the structure and composition of samples. Analyses indicate that the C-doped WO_3 nanoparticle cluster arrays are arranged in a beautiful hexagonal configuration and they are interconnected by a superthin carbon film. The cluster with sizes in the range of 12-15nm is composed by several 4-6nm nanocrystallines. An improved room temperature hydrogen response is found on C doped WO_3 nanoparticle cluster arrays, whose response sensitivity (S), response time and recovery time are 114, 162s and 108s, respectively. Three aspects are used to analyze reasons of the improved room temperature hydrogen response, which indicates that it has a great potential to develop the block copolymer based method to prepare excellent WO_3 based room temperature H_2 sensors.

1. Introduction

The microphase separation of block copolymers into periodic nanoscale structures are used as candidates for nanofabrication processes at length scales below those accessible by typical conventional top-down techniques.[1,2] Furthermore, the variety of morphologies available and the easy-tailoring sizes and periodicity make them ideal candidates as templates and scaffolds for the fabrication of nanostructured materials. Including ZnO[3], TiO_2[4], Cr[5], Pt[6] and et al, a lot of inorganic nanostructures have been reported to be prepared by block copolymer based methods. For example, a quick protocol for the fabrication of toroidal ZnO nanostructures is presented by Kim et al. taking block copolymer as templates.[3] Park et al. have ever used block copolymer templates to fabricate highly ordered gold and gold/silver composite arrays and found that they show characteristic local surface plasmon resonances. [7] An ultrahigh-density array of Ag nanoclusters for a SERS substrate with high sensitivity and excellent reproductivity at a large area are reported to take PS-b-P4VP as templates by Kim et al.[8] As one potential low cost sensing material WO_3 based nanostructures have high sensitivity and fast response for H_2 while its fabrication with block copolymers as templates has rarely been reported. Including hierarchical flowers [9], nanodots arrays [10], nanowires [11] , etc. a variety of WO_3 structures are prepared by such methods as hydrothermal synthesis, electrochemical anodizing, CVD and et al. Owing to the strong correlations between structures and sensing properties WO_3 based sensors with improved H_2 response abilities are hopefully to be achieved through designing the compositions, sizes and structures. Considering the numerous advantages offered by block copolymer based self-assembly, it is of great significance to make this method more widespread and accessible in preparation of WO_3 based hydrogen sensing fields.

Nowadays, main efforts in H_2 sensor development using WO_3 are focused on improving sensitivity at a lower operating temperature, especially at room temperature (RT). This target is initiated by the fact that conventional metal oxide (MOx)-based H_2 sensors require high Ts ~ 500℃. In this temperature range, an annealing effect would take place on the sensing material, which would result in changes of structure and/or composition. Additional requirements include safer detection of H_2, lower power consumption and miniaturization and scalability in production. However, higher activation energy at lower temperatures makes

[a][b] Dr. S. J. Liu, Prof. Dr. Y. Wang, Mr. Y. Yuan, Mr S. L. Zheng.

[a] School of Materials Science and Engineering, Harbin Institute of Technology, Harbin 150001, P. R. China

[b] Key Laboratory of Micro-Systems and Micro-Structures Manufacturing, Ministry of Education, Harbin 150001, P. R. China

E-mail:liusj0817@hit.edu.cn,y-wang@hit.edu.cn;Fax: (+86)0451-86402716

[c] Mr. J.H. Zhang.

Key Laboratory of Superlight Materials & Surface Technology, Ministry of Education, Harbin Engineering University, Harbin 150001, China

Supporting information for this article is given via a link at the end of the document.

Table 1. H_2 sensing performance of WO_3 based films produced by various methods: BCM (Block copolymer based methods), RFMS (R.F. magnetron sputtering), FSP (flame spray pyrolysis), RFS (radio frequency sputtering), SCBD (supersonic cluster beam deposition), EA (electrochemical anodising).

Material	Method	C_{H2}/ppm	Sensitivity(S)	t_{Res}/S	t_{Rec}	Operating temperature/℃	Ref.
C-WO_3	BCM	60000	114	162	108S	RT	This study
C-WO_3	BCM	60000	39	182	110S	RT	
WO_3:Au	RFMS	10000	350	72	115S	262	13
Pt-WO_3	FSP	10000	1.34×10^5	60	11min	150	14
Pt-WO_3	RFS	200	26	270	>30min	95	15
Pd-WO_3	Sol-gel	1300	2.5×10^4	100	60min	RT	12a
Pd/SCBD WO_3	SCBD	3000	1200	15	~30min	RT	16
SCBD WO_3	SCBD	20000	13	5220	---	RT	16
WO_3	EA	1000	103	1700	---	RT	10

the hydrogen response be hindered. To obtain an improvement in sensitivity at RT, addition of precious metals (Pt, Pd, Au) seems to be indispensable according to the researches.[12] On one hand, addition of an appropriate amount of metal additives promotes chemical reactions by reducing the activation energy between the film surface and the target gas. On the other hand, it increases the response and selectivity as well as decreasing the maximum temperature of sensor response. Table 1 summarizes the values of sensitivity (S), response time (t_{Res}), recovery time (t_{Rec}) and operating temperatures for some typical WO_3 based resistive hydrogen sensors produced by various methods.[13,14,15,16] It is found that the hydrogen response properties of samples has close relationships with the preparation methods and none of the hydrogen sensors meet all the requirements, including high sensitivity, low operating temperature and fast response and recovery. And all these are essential parameters for an outstanding hydrogen sensor. Moreover, addition of precious metal seems to be absolutely necessary, albeit it deviates the intention of the fabrication of a reliable and inexpensive H_2 sensor. Therefore, it is necessary to develop a facile and economic method to prepare WO_3 based RT high sensitivity and fast response and recovery sensors without addition of precious metals, which has been rarely reported.

Considering the strong correlations between structures and properties we wonder whether a low-cost WO_3 based RT H_2 sensor can be achieved just through designing its compositions, sizes and structures without addition of precious metals. As reported, when the unit size decreases to two times of its maximum thickness of the depletion layer, usually around 6 nm, the largest resistance response can be achievable.[17] Hence, sensors with sizes close to that critical value usually exhibit an increased hydrogen response. For example, a self-ordered array of WO_3 nanodots (50nm) composed of 9nm nanocrystallites is detected by Llobet et al. having high sensitivity to H_2 in the range of low H_2 concentrations.[18] The fabrication of such WO_3 nanodot-based hydrogen sensors involves a complex process of electrochemical anodising assisted by a nanoporous anodic alumina layer. Moreover, doping with extrinsic elements such as C is another effective way to improve gas-sensing performance toward target gases. It has been demonstrated that doping could introduce some new intragap bands and cause the band gap of metal oxides narrowing. The narrower the band gap, the lower the required energy for the transition of electrons from the valence to the conduction band. Zeng etc have reported that through doping with C, the band gap of WO_3 can be narrowed from 2.45eV to 2.12eV and subsequently the C-doped WO_3 sensor can detect 50ppb toluene at a low temperature of 90℃. [19] Lastly, formation of heterostructures is also beneficial for the improvement of gas response at lower operating temperature due to the depletion layer change in the heterojunctions. Taking the WO_3/multi-walled carbon nanotubes heterojunctions as an example, several groups have reported its increased hydrogen sensing performance at relative low temperatures.[20] In sum, it is possible to obtain WO_3 based room temperature sensors through designing the size, structure and composition accordingly by a proper method. Block copolymer based self-assembly methods would be such an ideal choice considering its characteristics of abundant structures and easy-tailoring nanosizes.

Herein, taking self-assembly structures of PS-b-P4VP as templates WO_3 based nanostructures including nanoparticle

cluster arrays and nanorods are prepared and the overall processes are described in Scheme 1. Including spin coating, solvent annealing, immersing in the mixed precursor solution, exposing to UV irradiation and calcinations, several steps are adopted to prepare the WO_3 based nanostructures.

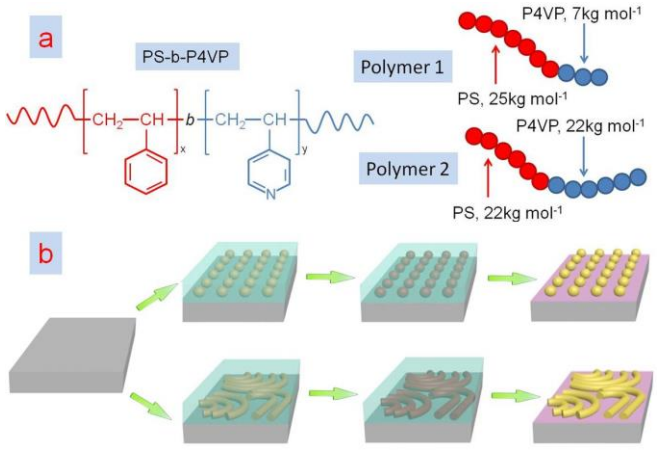

Scheme 1. a) Structure and molecular weight of the PS-b-P4VP used in this study. b) Schematic representation of C-doped WO_3 Nanostructures preparation with PS-b-P4VP.

2. Experimental Section

Materials. Block copolymers of poly(styrene-b-4-vinylpyridine) (PS-b-P4VP) with two different molecular weights(Polymer 1: PS(25k)-P4VP(7k), Mw/Mn=1.14 and Polymer 2: PS(22k)-P4VP(22k), Mw/Mn=1.07) were purchased from Polymer Source. Other reagents including ethanol, toluene, Na_2WO_4, HCl, etc were purchased from Sinopharm Chemical Reagent Co., ltd. All the reagents were used without further purification.

Preparation of Samples.

(1) Preparation of templates: Polymer 1 of PS(25k)-P4VP(7k) was dissolved directly in toluene at room temperature to yield a 0.6wt% solution. While the solution of polymer 2 (PS(22k)-P4VP(22k)) was first dissolved in toluene at 70℃ and then cooled down to room temperature to yield a 0.5wt% solution. Then the films of polymers were prepared by spin-coating a proper amount of polymers solution onto the silicon substrates. The film of polymer 1 was obtained at 2000 rpm for 30s, while that of polymer 2 was achieved at 3200rpm for 30s. After that the thin film of polymer 1 is used as templates of nanoarrays directly. While that of polymer 2 need to be exposed to tetrahydrofuran (THF)/ethanol (volume ratio 1:1) vapors for 40 hours at room temperature.

(2) Preparation of WO_3 based samples: After the self-assembly process completed, both films were immersed in the mixed aqueous solution (0.3% HCl and 2.6wt% Na_2WO_4) for 20min. Then the films were rinsed with deionized water to remove excess solution on the surface and placed in a drying oven at the temperature of 60℃. Afterwards, exposure to UV irradiation is undergone for twenty minutes. At last, the sample is calcined in a tube furnace at different temperatures for 1h with a controlled heating rate of 1℃/ min.

Fabrication of gas sensors.

Au film is produced as electrodes on the edge of the WO_3 based films through sputter coating. Then copper wires are jointed with Au electrodes by silver conductive adhesive. Afterwards, the devices are placed in a sealed container and then connected with the electrochemical workstation. The hydrogen response is tested using I-t mode through detecting the current change of hydrogen sensors at different atmospheres.

Characterization. The morphologies of the samples were investigated by atomic forced microscopy (AFM, Veeco, USA) operating in tapping mode and transmission electron microscopy (TEM). The ingredient of samples was determined by X-ray photoelectron spectroscopy (XPS, PHI 5700 ESCA, USA) with an Al Kα (1486.6 eV) source operated at 13 kV and 300 W. Hall effect is tested by a hall effect measurement system of Swin HALL8800. The hydrogen response is tested on the electrochemical workstation of CHI630E from Chenhua Company of Shanghai.

3. Results and Discussion

3.1 Film structure and composition

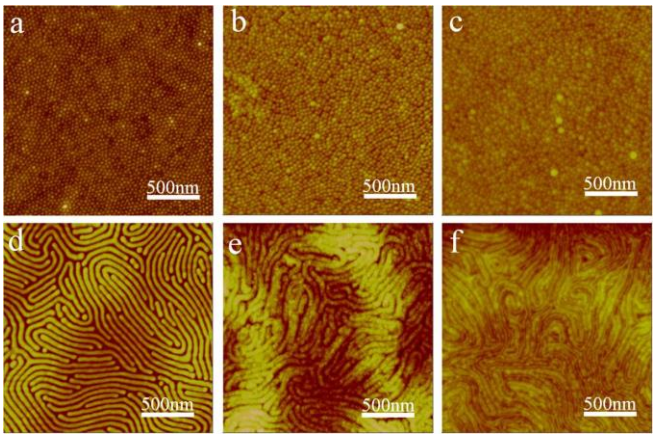

Figure 1. AFM images (height mode) of (a),(d) PS-b-P4VP template (b), (e) the template after immersed in H_2WO_4 solution (c) (f) WO_3 nanostructure.

As indicated in Figure 1 a series of AFM images (height mode) taken from the samples prepared following the scheme 1 above are shown clearly. Figures 1a,b,c and 1d,e,f are the transformation structures of PS-b-P4VP templates, templates immersed in the precursor solution and final WO_3 for two samples, respectively. In the whole process, fabricating self assembling structure of PS-b-P4VP is the first and most important step, which directly determines the final structures of WO_3. As indicated in Figure 1a,d two self-assembling structures of PS-b-P4VP are shown clearly, in which lighter areas are corresponded to the P4VP phase, while darker one is PS matrix. Observed from Figure 1a, a highly ordered lattice structure is presented and the size of nanodots is about 20±5nm. And the

center-to-center distance of two spheres is approximately 40±5nm. In comparison with this another PS-b-P4VP self-assembles into fingerprint structures composed by cylinders. The center-to-center spacing of the cylinders is approximately 30±4nm and the cylinder domains are a few hundreds of nanometers to micrometers in length (Figure 1d). From the AFM results, it can be concluded that two PS-b-P4VP self-assembling structures, highly ordered nanodots and fingerprint like nanorods are obtained here. Taking the PS-b-P4VP structures produced above as templates, structures of samples treated by several steps are demonstrated. Figure 1b, e show structures of block copolymer templates immersed with WO_4^{2-} and HCl aqueous solution for 20min. It can be seen that brief soaking of the PS-b-P4VP structures and subsequent rinsing in deionized water result in the diameters increase of the P4VP blocks due to the selective protonation and swelling.[6] Albeit with increasing sizes, the template structures are maintained completely. Subsequently, after UV exposure and removal of the block copolymer template by calcination two WO_3 based nanopatterns, highly ordered nanoparticle cluster arrays and fingerprint like structure composed by nanorods are obtained successfully. Compared with the PS-b-P4VP, WO_3 based samples nearly replicate its structure completely (Figure 1c and Figure 1f). While for its exact size, further TEM characterization shows clearly in the following part considering the AFM tips radius effects.

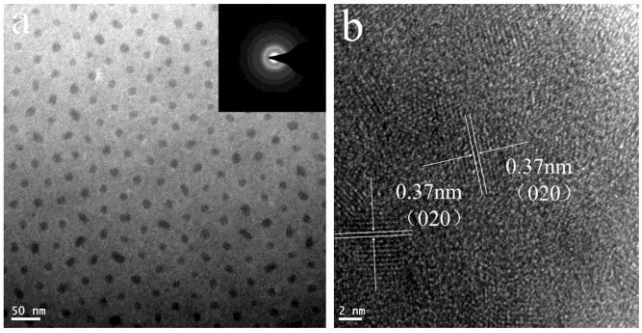

Figure 2. (a) TEM image and (b) High-resolution TEM image of WO_3 nanoparticle cluster arrays (inset: SAED pattern).

As another available data, the exact size and composition of nanoparticle cluster arrays in Figure 1c are verified further in Figure 2 by TEM images. As shown in Figure 2a, regular nanoparticle clusters arrays whose unit sizes are in the range of 12-15nm are distributed evenly on the film. The center-to-center distance of two adjacent nanoparticle clusters is approximately 41-46 nm. Moreover, they are arranged in a beautiful hexagonal configuration. Compared with the observation from AFM images, TEM results are more credible to reflect the sample sizes considering the existence of AFM tips radius effects. The corresponding high resolution TEM (HRTEM) image (Figure 2b) indicates further that a single cluster is composed of several 4-6nm grains, which is the just right size with the largest hydrogen response.[17] And the lattice fringes spacing is about 0.37nm, which is consistent with that of (020) planes of orthorhombic WO_3. In addition, a small quantity of separate nanocrystallines can be found among clusters occasionally. Such structure resembles the one reported by Llobet et al. exactly, that is a self-ordered WO_3 nanodots array composed of nanocrystallites. [18] Considering the similar structure, a highly ordered nanoparticle cluster array

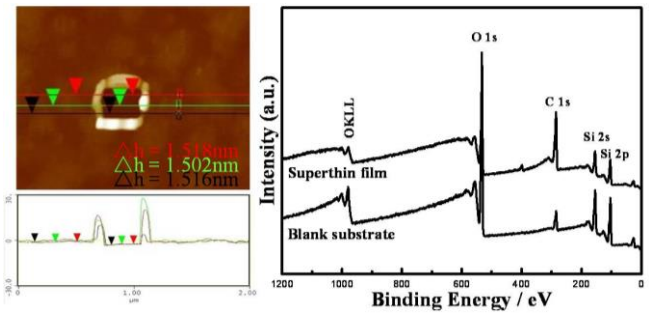

Figure 3. The remaining carbon film after calcination of pure block copolymer: a) A hole scratched by AFM tips; b) XPS spectra recorded.

composed of even smaller nanocrystallites (4-6nm) it is reasonable to bank on an improved hydrogen performance as reported. In a word, taking the phase separation structures of PS-b-P4VP block copolymers as templates WO_3 based nanoparticle cluster arrays with a regular hexagonal configuration is obtained facilely.

To make clear whether there exists something unseen to connect two adjacent clusters, which determines the hydrogen response mechanism subsequently, a control experiment is taken on a blank PS-b-P4VP film. This film experienced the same calcination treatment with the WO_3 based sample while without WO_4^{2-} ions loading. The hole scratched by AFM tips on this film (Figure 3a) shows that after calcinations in air at 450℃ for 1h, a superthin film with average thickness of about 1.5nm still exists. And it means that the seemingly separated WO_3 nanoparticle cluster arrays are in fact interconnected by this superthin film. XPS analyses (Figure 3b) are used to show the ingredient of this superthin film. In comparison with the blank substrate, all the peaks of Si, C and O peaks exist on the superthin film and the relative C amount with Si in the same curve is increased, which indicates the essence of C film. Rough estimates according to the resistance of substrate and this film also prove our deduction, whose value is consistent with that of C film. Hence, it is obvious that the calcination treatment can't wipe off all C element, not only can it form a superthin carbon film to connect the seemingly isolated WO_3 nanoparticle clusters, but also the carbon element should be left in the WO_3 nanocrystallines and forms C-doped WO_3. Therefore, both C doping in the WO_3 nanoparticles and heterojunctions formation between superthin carbon film and C-doped WO_3 nanoparticles are achieved here through this block copolymer based method facilely, which should have beneficial effects for the improvement of hydrogen response at ambient temperature.

To analyze the C doping condition, X-ray photoelectron spectroscopy (XPS) analysis was applied to the samples further. XPS high-resolution spectra of C1s, W4f and O1s core levels for the samples as-prepared and commercial WO_3 are shown in Figure 4 clearly. The detailed binding energies peaks of C1s, W4f and O1s are summarized in Table 2. In the C1s spectra, both the

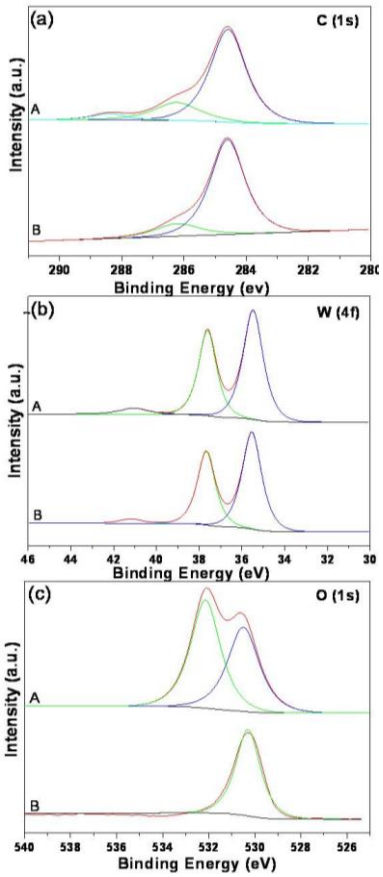

Figure 4. XPS high resolution spectra for (a) C1s, (b) W4f, (c) O1s core levels: A. As-prepared WO_3 sample; B. Commercial WO_3.

Table 2. Binding energies for C 1s, W4f , and O1 s core levels in as-prepared sample and commercial WO_3 powders

Samples	C1s (eV)			W4f (eV)		O1s (eV)	
As-prepared sample	284.6	286.2	288.2	35.42	37.55	530.5	532.1
Commercial WO_3	284.6	286.2	---	35.54	37.66	530.3	---

peaks at 284.6 eV and 286.2 eV can be detected in the as-prepared film and commercial WO_3. These peaks can be attributed to the presence of carbon-containing contamination which is unavoidable for all air exposed materials. Compared with the commercial WO_3, the peak located at 288.2 eV can be observed only in the sample as prepared. It indicates that carbonates species are present in the system and most doped carbon atoms are bonding to O atoms forming CO-like species.[i] In addition, no peak is visible at around 281eV, suggesting W-C bonds are not formed in our samples. In the W4f spectrum, the peak positions centered at 35.42 and 37.55 eV can be associated with the binding energy of W4f7/2 and W4f5/2 for the sample as prepared. While that of commercial WO_3 are located on the positions of 35.54 and 37.66 eV. In the O1s spectrum, both the peak centered at 530.5 eV of as-prepared sample and 530.3 eV of commercial WO_3 can be attributed to the lattice oxygen in the WO_3 crystal. The binding energy of 532.1eV of as-prepared film can be ascribed to the hydroxyl groups or water bonded on the film surface.[22] Based on the results that no obvious binding energy shifts in W4f and O1s peaks it can be concluded that the doped C should located at interstitial sites.[23]

3.2 Hydrogen response

From the results above it can be concluded that a special structure with C-doped WO_3 nanoparticle cluster arrays interconnected by a superthin C film is obtained facilely with block copolymer as templates. Three aspects including C doping, formation of heterostructures and highly ordered nanoparticle cluster arrays with nanocrystallines sizes of 4-6nm are mentioned in the structure, which are beneficial for the improvement of hydrogen sensing at low temperatures. To evaluate the sensor performance quantitatively, the sensor sensitivity (S) is defined as I_0-I/I, which is equivalent to the definition based resistances of R-R_0/R_0 (I and R are the current and resistance of films in H_2, I_0 and

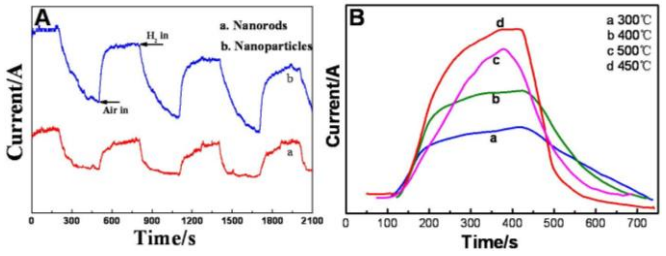

Figure 5. Response of C-doped WO_3 hydrogen sensors at room temperature for 6% H_2: A) Samples with different structures; B) Samples of nanoparticle cluster arrays calcinated at different temperature.

R_0 are that in air). The response time of the sensor is defined as the time required for the current to reach 90% of the equilibrium value following exposure to H_2. The recovery time is the time necessary for the current to return to 10% above original current after removal of H_2. Figure 5A shows the sensor response of the nanoparticle cluster arrays and nanorods based WO_3 samples toward 6% H_2 at room temperature. The corresponding experimental results indicate that the response time and recovery time of nanoparticle cluster arrays are 162s and 108s, while that of the nanorods based WO_3 samples are 182s and 110s, respectively. Moreover, the sensitivity of nanoparticle cluster arrays (S=114) is about three times higher than that of nanorods (S=39). The differences of hydrogen response between nanoparticle cluster arrays and nanorods should be derived from a larger BET surface area of nanoparticle cluster arrays and will be explained in the following hydrogen mechanism part. Compared with other sensors reported (Table 1), although the sensitivity S cannot catch some of them, it still should deserve praise for its fast response and recovery at RT without addition of precious metals, which is an evaluable attempt for this block copolymer based method. Further improved response is promising to be achieved through optimizing experiment conditions.

To make further investigation hydrogen responses of samples calcined at different temperatures, in which the residual carbon amount varies with the calcining temperature, are tested in detail.

As indicated in Figure 5B, the sample obtained at 450 ℃shows the best hydrogen response sensitivity (S=114), meanwhile, it shows the shortest response time of 162s. All three other C-doped WO_3 based sensors show inferior hydrogen response, no matter the samples calcined at high or low temperatures, which proves the significance of treatment temperature. As we imagined, the residual carbon amount varies with the treating temperature due to its function of decomposing PS-b-P4VP templates. Thus here, considering the variation of hydrogen response with calcination temperatures, a suitable remaining amount of carbon both on the substrate and in the C-doped WO_3 nanoparticles plays a significant role for the improved hydrogen response. The detailed mechanism will be discussed later.

Table 3. The hall effect of C-doped WO_3 nanoparticle cluster arrays

Carrier concentration(cm^{-3})	Mobility(cm^2/Vs)	Resistivity(Ω·mm)
3.237731E+15	3.427041E+2	5.625115E-1

Moreover, observations from the hydrogen response above indicate that it varies from other WO_3 based sensors and the resistance will decrease in the air, which is a distinct character of p-type semiconductor. To make clear this Hall Effect is tested and the result indicates (Table 3) that Hall coefficient of RH is positive, which proves the essence of p-type semiconducting behavior. It is a direct evidence for the p-type performance of hydrogen response of this WO_3 based sensors. According to reports, [20] through doping with extrinsic elements or formation of heterostructure with other materials a hybrid film can exhibit as either p-type or n-type depending on the doping quantity or the operating temperature. Here both conditions of doping with extrinsic element and formation of heterostructures exist, which makes it behave as a p-type semiconductor reasonably. The exact explanation for this behavior is provided in the next mechanism part.

3.3 Hydrogen sensing mechanism

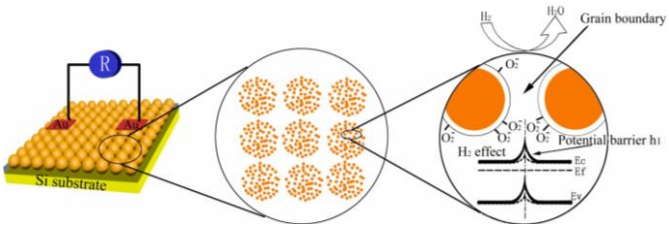

Scheme 2. The sensing mechanism of the C-doped WO_3 nanoparticle cluster arrays sensors to H_2.

It is well known that the essence for detection of inflammable gases is catalytic oxidation of target gas over the grain surface. [24] The gas sensing abilities of semiconducting metal oxides are attributed to the chemisorptions of ionic oxygen species, such as O_2^-, O^-, and O_2^- (which is decided by the temperature). At room temperature, the adsorbed ionic oxygen species is mainly dominated by O_2^- ions forms (533.9eV). [25]

$O_2+e^- = O_2^-$ (1)

This process creates a space-charge layer on the surface of particles (Scheme 2) and subsequently an increased Schottky potential barrier (h_1) is resulted in. According to the experimental analyses the sensor prepared has a structure with C-doped WO_3 nanoparticle cluster arrays interconnected by a superthin carbon film. Due to the lower work function of WO_3 (~4.30eV) than that of C (~4.81eV), electrons transfer from C-doped WO_3 nanoparticles to carbon films at the heterojunctions, thereby creating accumulation of electrons in the carbon film. Therefore band bending occurred in WO_3 to realize charge balance between the semiconductor and the carbon film. Hence another depletion layer and increased Schottky barrier (h_2) are created at the interface between C-doped WO_3 nanoparticles and carbon films (Scheme 3). According to the report [26] by Hu et al., a large amount of adsorbed oxygen species on the surfaces is beneficial to realize stabilization of the unstable surface states. Considering the large amount of adsorption sites of nanocrystallines high concentration of oxygen species can be adsorbed on the surfaces, which result in the band bending further enlarged and the position of Ei rising. When Ei is increased above Ef, it means that holes have become the majority charge carriers [27] and the surface conduction type transformed from n-type to p-type. Scheme 3 shows the energy-level diagram of the C-doped WO_3 nanoparticles affected by the formation of heterostructures with C film. When exposed to H_2 gas, the space charge layer can be eliminated due to the reaction of H_2 with the surface-adsorbed O_2^- ion, thus releasing the electron back to the conduction band of WO_3.

$2H_2 + O_2^- = 2H_2O + e^-$

Considering that the majority charge carrier are holes here, the resistance of sensor will increase in accompany with the introduction of H_2. As a result, a WO_3 based sensor with p-type performance is obtained here.

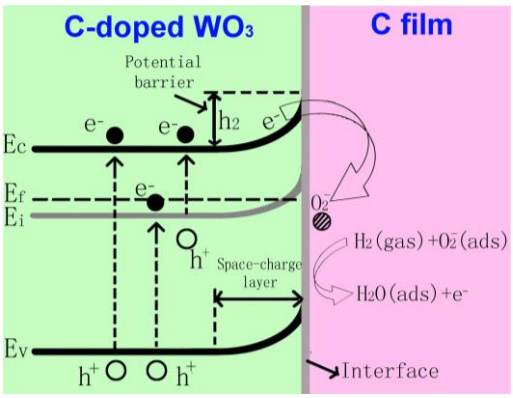

Scheme 3. Schematic diagram showing the energy band structure of C-doped WO_3 affected by heterostructures formation.

Generally, semiconducting oxide gas sensors operate on the basis of the conductivity changes due to the electrons transfer between sensing material and test gas. The alteration of gas concentration and species will lead to a modification of the space-charge layers. Subsequently the height of potential barrier, then the conductivity and the H_2 response will be determined. According to the analyses above, two different depletion layers and associated potential barriers coexist in this structure. One is

located on the surfaces of the C-doped WO_3 nanoparticles (h_1) and the other is in the interface of heterostructures (h_2). Both the barriers play an important role in the overall conductivity of the gas sensitive WO_3 based film. The superimposed effects of these two changes should be one significant aspect for the increase of the room temperature response of the WO_3 based hydrogen sensors. Besides, in the structure the superthin carbon film plays a role of interconnecting the particles and hence forms a new conducting way. When encountering H_2 the conductance modification of each C-doped WO_3 nanoparticle will be transmitted quickly through this new conducting pathway and consequently an improved hydrogen response is achieved. It indicates that the superthin carbon film here has the similar conducting function with WO_3 nanosized gaps as reported. [18]

Moreover, carbon doping which exist as carbonates species would be another beneficial factor for the improvement of hydrogen response. According to the report carbonates species present in the system indicate most doped carbon atoms are bonding to O atoms forming CO-like species. The paired C and O atoms make the energy of most O 2p levels and part of C 2p levels largely reduced due to the coupling interaction, which accounts for the total energy reduction and subsequently induces an effective band gap reduction. [21] Then low activation energy would be enough to make electrons transition from the valence band to conduction band. Zeng et al have reported that C-doped WO_3 microtubes can have ultrahigh sensitivity to toluene at low operating temperature of 90℃ just through doping with C. [19] Therefore, it is reasonable for us to believe that doping with C element here is one significant reason for the excellent hydrogen response at ambient temperature. According to the analyses above, both doping with extrinsic elements of carbon and formation of superthin carbon film are beneficial for the improvement of sensing performance at ambient temperature. Annealing treatment is the key step to affect the amount and quality of residual carbon mentioned in the doping condition and carbon film. Therefore the fact that the hydrogen sensitivity of samples varies with the treating temperatures will support the mechanism that residual carbon is of great importance for the improved hydrogen response.

In addition, the structure of nanoparticle cluster arrays then complemented by the increased BET surface areas will be the third favorable factor for the improvement of the hydrogen sensing performance of WO_3 based sensors. According to reports, [17] the largest resistance response is achieved when the unit size (usually around 6 nm) is two times of its maximum thickness of the depletion layer. Here the nanoparticle cluster arrays have nanocrystallines with sizes of 4-6nm, which is the just right critical size as analysis indicated. Hence it is reasonable for us to attribute the improved hydrogen response at room temperature to the nanostructure. Moreover, due to the nanostructure more stoichiometric defects such as oxygen vacancies are present in the material to act as adsorption sites for gaseous species. Simultaneously, the smaller of a single nanoparticle the larger contact area between the nanoparticle and the carbon film. Consequently more space charge layer and much faster conductance transmission will emerge and finally an improved hydrogen response is obtained. The hydrogen response differences between nanoparticle cluster arrays and nanorods obtained by a similar method here would prove the analysis above further. The corresponding AFM images indicate that nanorods (30±3.7nm in diameters and a few hundreds of nanometers to micrometers in length) have larger sizes than nanoparticles (diameters in 20±4.7nm). Its corresponding BET surface area should be smaller than that of nanoparticle cluster arrays. Therefore less adsorption sites for gaseous species, less space charge layer between heterostructures and thus worse hydrogen response are obtained on the WO_3 nanorods based film.

4. Conclusions

In summary, C-doped WO_3 based hydrogen sensors including nanoparticle cluster arrays and nanorods have been synthesized taking PS-b-P4VP self-assembly structures as templates and used in room temperature hydrogen response. Analyses indicate that the C-doped WO_3 nanoparticle cluster arrays are interconnected by a superthin carbon film. The C-doped WO_3 nanoparticle cluster arrays have cluster sizes in the range of 12-15nm and center-to-center distances approximately 41-46 nm. In addition, they are arranged in a beautiful hexagonal configuration. Each cluster is composed by several nanocrystallines with sizes of 4-6nm. It is found that the C-doped WO_3 nanoparticle cluster arrays based hydrogen sensor exhibit a high response sensitivity (S=114) to hydrogen at room temperature. Three aspects are used to analyze the reasons of room temperature hydrogen response, including the formation of nanostructures, doping with extrinsic elements of C, formation of heterostructures between C-doped WO_3 nanoparticles and carbon film. The responses differences of samples calcinated at different temperatures and samples with different morphologies (nanoparticle cluster arrays and nanorods) are the strong experimental evidences to support the conclusion. The successful integration of positive aspects for improving hydrogen responses through this facile block copolymer based method would provide a new way for the development of excellent WO_3 based room temperature H_2 sensors further.

Acknowledgements

This work is funded by 973 Program (2012CB934100), National Natural Science Foundation of China (21101043), Research Fund for Doctoral Program of Higher Education of China (20112302120018), Special Research funds for Scientific and Technical Innovative Talents of Harbin City (2012RFQXG108), the Key Laboratory Fund of HIT, and Interdisciplinary Basic Research of Science-Engineering-Medicine in HIT.

Notes and references

1 a) C. A. Ross, K. K. Berggren, J. Y. Cheng, Y. S. Jung, J. B. Chang, *Adv. Mater*. 2014, **26**, 4386. b) R. Ruiz, H. Kang, F. A. Detcheverry, E. Dobisz, D. S. Kercher, T. R. Albrecht, J. J. Pablo, P. F. Nealey, *Science* 2008, **321**, 936.

2 S. Park, B. Kim, A. Cirpan, T. P. Russell, *Small* 2009, **5**, 1343.

3 Y. H. Jang, S. Y. Yang, Y. J. Jang, C. Park, J. K. Kim, D. H. Kim, *Chem. Eur. J*, 2011, **17**, 2068.

4 P. S. Chinthamanipeta, Q. Lou, D. A. Shipp, *Acs Nano*, 2011, **5**,

450.

5 A. J. Hong, C. C. Liu, Y. Wang, J. Kim, F. X. Xiu, S. X. Ji, J. Zou, P. F. Nealey, K. L. Wang, *Nano Lett.* 2010, **10**, 224.

6 J. N. Chai, D. Wang, X. N. Fan, J. M. BURIAK, *Nature Nanotechnology* 2007, **2**, 500.

7 P. A. Mistark, S. Park, S. E. Yalcin, D. H. Lee, O. Yavuzcetin, M. T. Tuominen, T. P. Russell, M. Achermann, *Acs Nano*, 2009, **3**, 3987.

8 W. J. Cho, Y. Kim, J. K. Kim, *Acs Nano*, 2012, **6**, 249.

9 C. Wang, R. Z. Sun, X. Li, Y. F. Sun, P. Sun, F. M. Liu, G. Y. Lu, *Sens. Actuators B* 2014, **204**, 224.

10 R. Calavia, A. Mozalev, R. Vazquez, I. Gracia, C. Cané, R. Ionescu, E. Llobet, *Sens. Actuators B* 2010, **149**, 352.

11 a) J. Zhou, Y. Ding, S. Z. Deng, L. Gong, N. S. Xu, Z. L. Wang, *Adv. Mater.* 2005, **17**, 2107. b) L. F. Zhu, J. C. She, J. Y. Luo, S. Z. Deng, J. Chen, N. S. Xu, *J. Phys. Chem. C* 2010, **114**, 15504.

12 a) S. Fardin, I. Z. Azam, F. Rahimi, E. R. Ghas, *Int J Hydrogen Energy* 2010, **35**, 854. b) M Ando, R Chabicovsky, M. Haruta, *Sens. Actuators B* 2001, **76**, 13. c) M. H. Yaacob, M. Breedon, K. Kalanta, W. Wlodarski, *Sens. Actuators B* 2009, **137**, 115. d) J. Y. Shim, J. D. Lee, J. M. Jin, H. Cheong, S. H. Lee. *Sol. Energy Mater. Sol. Cells* 2009, **93**, 2133. (f) J. Choi, J. Kim, *Sens. Actuators B* 2009, **136**, 92.

13 S. J. Ippolito, S. Kandasamy, K. Kalantar-zadeh, W. Wlodarski, *Sens. Actuators B Chem*, 2005, **108**, 154.

14 T. Samerjai, N. Tamaekong, C. Liewhiran, A. Wisitsoraat, A. Tuantranont, S. Phanichphant, *Sens. Actuators B* 2011, **157**, 290.

15 C. Zhang, A. Boudiba, C. Navio, C. Bittencourt, M. G. Olivier, R. Snyders, M. Debliquy, *Int J hydrogen energy* 2011, **36**, 1107.

16 M. Zhao, J. X. Huang, C. W. Ong, *Nanotechnology* 2012, **23**, 315503.

17 a) N. Yamazoe, Sens. Actuators B, 1991, 5, 7-19. b) M. E. Franke, T. J. Koplin, U. Simon, *Small*, 2006, **2**, 36.

18 R. Calavia, A. Mozalev, R. Vazquez, I. Gracia, C. Cané, R. Ionescu, E. Llobet, *Sens. Actuators B* 2010, **149**, 352.

19 X. H. Ding, D. W. Zeng, S.P. Zhang, C.S. Xie, *Sens. Actuators B* 2011, **155**, 86.

20 a) C. Bittencourt, A. Felten, E.H. Espinosa, R. Ionescu, E. Llobet, X. Correig, J. J. Pireaux, *Sens. Actuators B* 2006, **115**, 33. b) C. Wongchoosuk, A. Wisitsoraat, D. Phokharatkul, A. Tuantranont, T. Kerdcharoen, *Sensors* 2010, **10**, 7705. c) R. Ghasempour, A. I. zad, *J. Phys. D: Appl. Phys.* 2009, **42**, 165105.

21 J. B. Lu, Y. Dai, M. Guo, L. Yu, K. R. Lai, B. B. Huang, *Appl. Phys. Lett.* 2012, **100**, 102114.

22 S. R. Bathe, P. S.Patil, *J Phys D: Appl. Phys.* 2007, **40**, 7423.

23 Y. P. Sun, C. J. Murphy, K. R. Reyes-Gil, E. A. R. Garcia, J. M. Thornton, N. A. Morris, D. Raftery, *Int. J hydrogen energy* 2009, **34**, 8476.

24 a) G. Sakai, K. Shimanoe, *Catal. Surv. Asia*, 2003, **7**, 63. b) Y. R. Wang, B. Liu, D. P. Cai, H. Li, Y. Liu, D. D. Wang, L. L. Wang, Q. H. Li, T. H. Wang, *Sens. Actuators B* 2014, **201**, 351.

25 a) T. P. Chen, H. Y. Shih, J. T. Lian, *Opt. Express* 2012, **20**, 17136. b) N. Barsan, U. Weimar, *J. Electro-ceram*. 2001, **7**, 143.

26 M. D. Li, M. Hu, D. L. Jia, S. Y. Ma, W. J. Yan, *Sens. Actuators B* 2013, **186**, 140.

27 a) K. Galatsis, L. Cukrov, W. Wlodarski, P. McCormick, K. Kalantar-zadeh, E.G. Comini, *Sens. Actuators B* 2003, **93**, 562. b) A. Gurlo, N. Barsan, A. Oprea, M. Sahm, T. Sahm, U. Weimar, *Appl. Phys. Lett.* 2004, **85**, 2280.